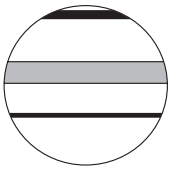

Research paper

The Holocene
1–12

DOI: 10.1177/0959683610369508
http://hol.sagepub.com
SAGE

Holocene climate change in arid Australia from speleothem and alluvial records

Mark C. Quigley,[1] Travis Horton,[1] John C. Hellstrom,[2] Matthew L. Cupper[2] and Mike Sandiford[2]

Abstract

New high-resolution MC-ICPMS U/Th ages and C and O isotopic analyses from a Holocene speleothem in arid south-central Australia provide evidence for increased effective precipitation (EP) relative to present at *c.* 11.5 ka and *c.* 8–5 ka, peak moisture at 7–6 ka, and onset of an arid climate similar to present by *c.* 5 ka. $\delta^{18}O$ and $\delta^{13}C$ time-series data exhibit marked (>+1‰) contemporaneous excursions over base-line values of −5.3‰ and −11.0‰, respectively, suggesting pronounced moisture variability during the early middle Holocene 'climatic optimum'. Optically stimulated luminescence and ^{14}C ages from nearby terraced aggradational alluvial deposits indicate a paucity of large floods in the Late Pleistocene and at least five large flood events in the last *c.* 6 kyr, interpreted to mark an increased frequency of extreme rainfall events in the middle Holocene despite overall reduced EP. Increased EP in south-central Australia during the early to middle Holocene resulted from (1) decreased El Niño-Southern Oscillation (ENSO) variability, which reduced the frequency of El Niño-triggered droughts, (2) the prevalence of a more La Niña-like mean climatic state in the tropical Pacific Ocean, which increased available atmospheric moisture, and (3) a southward shift in the Intertropical Convergence Zone (ICTZ), which allowed tropical summer storms associated with the Australian summer monsoon (ASM) to penetrate deeper into the southern part of the continent. The onset of heightened aridity and apparent increase in large flood frequency at *c.* 5 ka is interpreted to indicate the establishment of an ENSO-like climate in arid Australia in the late Holocene, consistent with a variety of other terrestrial and marine proxies. The broad synchroneity of Holocene climate change across much of the Australian continent with changes in ENSO behavior suggests strong teleconnections amongst ENSO and the other climate systems such as the ASM, Indian Ocean Dipole, and Southern Annular Mode.

Keywords

alluvial deposits, Australian summer monsoon, ENSO, Holocene climate change, Indian Ocean dipole, precipitation, Southern Annular Mode, speleothem

Introduction

Global ecosystems and human populations have been affected by changes in the frequency, magnitude and seasonal distribution of rain over the Holocene (Mayewski *et al*., 2004). Precipitation proxy data from the Holocene can provide insight into past connections between weather, climate and environments of relevance to understanding contemporary interactions. Additionally, paleoprecipitation data provide pre-industrial baselines upon which to assess whether changing rainfall distributions and magnitudes reflect anthropogenically influenced climate change (McInnes *et al*., 2003; Zhang *et al*., 2007). Speleothems (secondary $CaCO_3$ cave deposits) provide high-resolution proxy records of 'effective' moisture that can be related to long-term rainfall variability (e.g. Asmerom *et al*., 2007; Drysdale *et al*., 2006, 2007). Coarse alluvial terrace deposits provide evidence for large paleofloods and can be dated to determine paleoflood frequency (e.g. Keefer *et al*., 2003; Wells, 1990). By combining these approaches, past spatial and temporal relationships between effective moisture (e.g. mean annual precipitation, precipitation-evaporation indices) and moisture variability (e.g. large floods) can be resolved, with relevance for understanding the evolution of major climatic phenomenon such as ENSO (e.g. Gomez *et al*., 2004).

A variety of studies have identified the middle Holocene 'climatic optimum' (*c*. 8–5 ka) as the last time that many of Earth's most dominant climatic systems operated differently from present, providing an opportunity to examine the cause and effects of relatively recent dramatic climate change prior to global industrialization (Bond *et al*., 1997; Steig, 1999). ENSO variability was suppressed (e.g. Gomez *et al*., 2004; McGregor and Gagan, 2004; Rodbell *et al*., 1999; Tudhope *et al*., 2001) and a more La Niña-like mean climatic state, typified by warmer sea surface temperatures in the western Pacific, prevailed across the tropical Pacific Ocean (Koutavas *et al*., 2002). Cooler mean annual sea surface temperatures in the eastern Indian Ocean were manifest as strong Indian Ocean Dipole (IOD) events (Abram *et al*., 2007) and the Asian (Wang *et al*., 2005) and Australian (Griffiths *et al*., 2009; Singh and Luly, 1991) summer monsoons were stronger than present. Wetter conditions prevailed over much of northern and eastern Australia (McGlone *et al*., 1992; Shulmeister and Lees, 1995), however the extent to which the southern parts of the continent were wet

[1]University of Canterbury, New Zealand
[2]The University of Melbourne, Australia

Received 9 October 2009; revised manuscript accepted 15 March 2010

Corresponding author:
Mark C. Quigley, Department of Geological Sciences, University of Canterbury, Christchurch, New Zealand
Email: mark.quigley@canterbury.ac.nz

(e.g. McCarthy and Head, 2001; Stanley and De Deckker, 2002) or dry (Marx *et al*., 2009) are debated. Improved high-resolution climate records from south-central Australia are required to better constrain the influence of middle-Holocene climate change on this environmentally sensitive region.

The onset of the modern ENSO-dominated climate, typified by increased climatic variability as a result of more frequent and stronger El Niños, occurred *c*. 5 kyr ago (Haberle and Ledru, 2001; Rodbell *et al*., 1999; Sandweiss *et al*., 1996), coinciding with a decrease in Australian summer monsoon activity (Singh and Luly, 1991) and a general drying of the Australian continent (Cupper, 2005; Marx *et al*., 2009). ENSO presently exerts a strong influence on precipitation and precipitation variability across much of the Australian continent, either directly or indirectly via teleconnections with other components of the ocean–atmosphere system such as the Southern Annular Mode (SAM) (Meneghini *et al*., 2007), Indian Ocean Dipole (IOD) (Saji *et al*., 1999) and Australian summer monsoon (ASM) (Allan, 1985).

In this study, we present new U/Th ages and C and O isotopic analyses from an extinct speleothem and optically stimulated luminescence (OSL) and ^{14}C ages from alluvial sediments (Quigley *et al*., 2006, 2007a; Williams, 1973) that reveal Holocene changes in EP and precipitation variability in the presently arid Australian interior. The study sites are situated in a region that presently lacks any strong seasonal variability in annual rainfall (Figure 1). However, on multiyear timescales, large spatial and temporal variations in precipitation occur because of ENSO activity, varying intensities of tropical air masses associated with the ASM, and changes in the position and intensity of middle and high latitude frontal systems associated with changing sea surface temperature gradients in the eastern Indian and Southern Oceans (Evans *et al*., 2009; McInnes *et al*., 2003; Meneghini *et al*., 2007). The paleoprecipitation data presented herein provide insight into the behavior and interactions of these climatic phenomena over the Holocene.

Study sites: Locations, descriptions and justification

The Flinders Ranges form part of a rugged upland system extending from the southern Australian coast south of Adelaide to the Lake Eyre Basin in the north (Figure 1). The ranges are flanked by lowland piedmonts comprising colluvial, alluvial and aeolian deposits with intercalated paleosols and large, internally draining playa lake basins (Lakes Frome, Eyre and Torrens). Mean annual precipitation across the region is low (<310 mm/yr) and only weakly seasonal. The speleothem site has a summer (December–February) to winter (June–August) rainfall ratio of 2.1:1 while the alluvial fan site has a summer–winter rainfall ratio of 1:1.4 (Figure 1). Summer rainfall is commonly associated with southward incursions of tropical northerly systems (Schwerdtfeger and Curran, 1996), while winter rainfall is dominantly supplied by extra-tropical cyclones and cold fronts originating in the Indian and Southern Oceans (Evans *et al*., 2009; Meneghini *et al*., 2007). Precipitation is strongly influenced by topography, with surrounding piedmonts and basins receiving less than 200 mm/yr and the high ridges receiving over 400 mm/yr. Rainfall is greatly exceeded by annual evaporation, accounting for the lack of permanent water bodies save a few small, spring-fed streams. However, during sporadic, intense summer rainfall events (e.g. 14 March 1989 event, 273 mm in 24 h in the Lake Torrens area; www.bom.gov) large streams

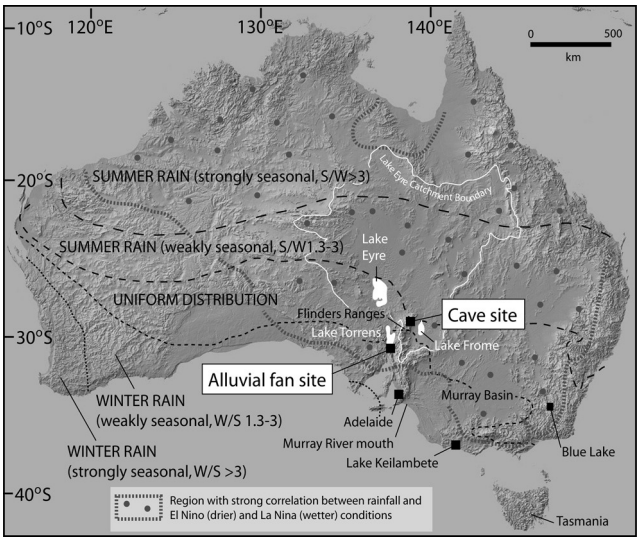

Figure 1. Map of Australian rainfall seasonality (Magee *et al*., 2004) and regions where historical winter/spring rainfall is influenced by El Niño (shift towards drier than average conditions) and La Niña (shift towards wetter than average conditions; modified from http://www.bom.gov.au /info /leaflets/nino-nina.pdf). S/W, summer to winter rainfall ratio; W/S, winter to summer rainfall ratio. Speleothem and alluvium sampling sites reside within the weakly seasonally winter rainfall zone in a region historically influenced by ENSO

transport coarse bedload, including boulders of >1 m diameter. Historical rainfall records reveal, in general, decreased precipitation or drought during strong El Niño events and increased precipitation during La Niña events, consistent with rainfall records across much of eastern Australia (Nicholls, 1992). The region experiences marked diurnal and seasonal temperature extremes, with average daily extreme of temperatures of 17–34°C in summer and 2–17°C in winter at the speleothem site (Sprigg, 1984).

The Yudnamutana speleothem was obtained from a ~10 m deep overhang cave (30°11′16″S, 139°24′58″E) elevated ~ 8 m above the adjacent Yudnamutana Creek in the northern Flinders Ranges (Figure 1). Yudnamutana Creek forms part of an antecedent, highly ephemeral drainage basin deeply incised (~600 m) into granite, gneiss and schist basement rocks that have been uplifted by thrust faulting along the tectonically active range front (Quigley *et al*., 2007c). The cave is situated within highly fractured, U-rich Proterozoic granite (Coats, 1973). Recharge throughout the ranges is limited to direct infiltration of rainfall through bedrock fracture networks, with the bulk of water discharge associated with small, fault-related springs (Brugger *et al*., 2005). The water-table in the ranges follows topography and lies up to ~9 m below the surface (Brugger *et al*., 2005), thus stream flow throughout the ranges is restricted to rare, infrequent flood events.

Within the Yudnamutana cave (Figure 2A), there is a cleft in the granite wall from which water has clearly flowed in the past. The cleft feeding this system has created a flowstone deposit with an area of ~0.25 m^2 on the wall beneath this outlet, of between about 10 and 40 mm in thickness (Figure 2B,C). We sampled the flowstone at its thickest point, with water probably channeled to, and flowing down, a ridge in the cave wall. Sample extraction revealed continuity of depositional units over its width and down onto the cave floor where they are interspersed with cave sediments. The position of the cave slightly above the creek floor beneath steep relief suggests that it provides a good proxy for

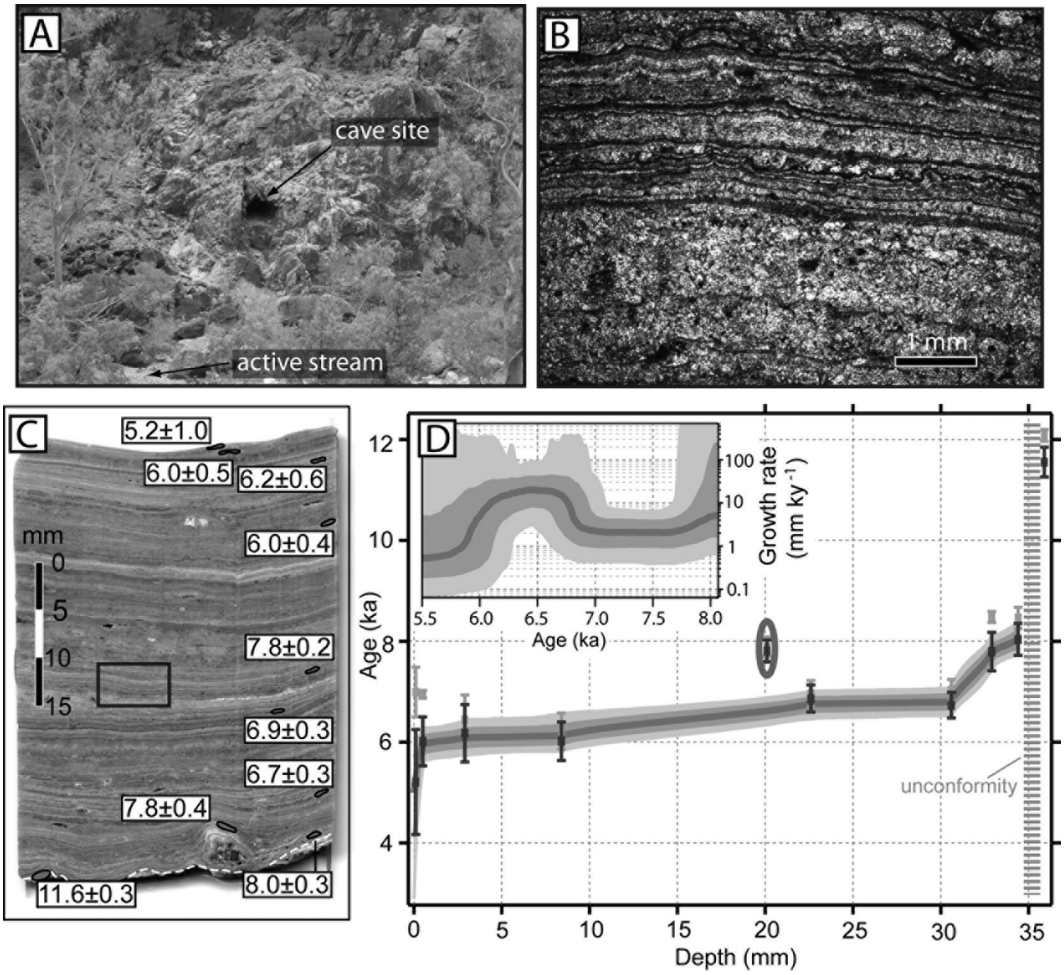

Figure 2. (A) Yudnamutana cave site, situated ~8 m above the active stream channel. (B) Laminated speleothem in section, showing compositional layering. Location of section shown by box in (C). (C) Laminated speleothem cross-section showing location of corrected U-Th spot ages. Dashed line, unconformity. (D) U-Th age versus depth plot, showing uncorrected (light grey) and corrected ages (dark grey) corrected for initial ^{230}Th using an initial $^{230}Th/^{232}Th$ ratio obtained from Paralana Hot Springs water. Uncertainty envelopes on monotonic age–depth curve, developed from all analyses baring the circled outlier, are 67% and 95%. Inset shows growth rate versus age plot. Note peak in growth rate between *c.* 7 and 6 ka

groundwater conditions, with speleothem growth associated with much moister conditions than prevail today. The presence of spring water in this cave could only be possible with a higher local water-table than at present, most likely intercepting the valley floor. It is thus likely that the adjacent Yudnamutana Creek was flowing at times that the spring was active.

The paleoflood record is derived from the Wilkatana alluvial fans on the western side of the west-central Flinders Ranges, roughly 270 km southeast of the cave site (Figure 1). This sample site was specifically selected because the fans have been extensively studied and dated using OSL and radiocarbon techniques (Quigley *et al*., 2007a,b; Williams, 1973) and are located in a geomorphic setting that is particularly favorable for capturing a depositional signal of large paleofloods. Favorable attributes include small (commonly < 20 km^2) and steep source catchments, which minimize sediment retention during large floods (Quigley *et al*., 2007b) and a tectonically active reverse fault along the range front (Quigley *et al*., 2006), which transports hillslope material to the streams via co-seismic landslides and generates accommodation space in the subsiding footwall basin, thus enhancing the development and preservation of depositional terraces proximal to the range front (Quigley *et al*., 2007b). Additional paleoclimate proxy data sets briefly described in this paper include sites from throughout much of the south-central and southeastern parts of Australia, including the Flinders Ranges, Lake Frome, Lake Eyre, Tasmania, Murray Basin and Lake Keilambete (Figure 1).

U/Th dating of the Yudnamutana speleothem

Sample description

The Yudnamutana speleothem consists of hundreds of 10–100 μm thick laminae ranging from clear, microcrystalline calcite-rich layers to red-brown and black layers rich in Fe-oxide, mica and smectitic clay (Figure 2B,C). Based on petrographic observation of the speleothem in thin section, the laminae compositional variability appears to reflect variations in the concentration of detrital impurities (Figure 2B). The lamina structure is dominantly parallel and continuous and ranges from relatively planar to wavy to bulbous. Individual laminations are able to be traced across the width of the section regardless of the laminae structure and, with one exception, are not truncated, suggesting that there were no major periods of

Table 1. U-Th activity ratio, age and depth data for the Yudnamutana speleothem sample

Sample	Depth (mm) [a] (± 2σ)	Mass [b] (g)	U [c] (ng/g)	$[^{230}Th/^{238}U]$ [d] (± 2σ)	$[^{234}U/^{238}U]$ [d] (± 2σ)	$^{232}Th/^{238}U] \times 10^3$ (± 2σ)	$[^{230}Th/^{232}Th]$ [d]	Age ka [e] (± 2σ)	$[^{234}U/^{238}U]_i$ [f] (± 2σ)
YC1.1	0.1 (0.1)	$<10^{-4}$	$>10^4$	0.0835 (0.0058)	1.338 (0.007)	2.136 (0.032)	39	5.2 (1.0)	1.342 (0.007)
YC001-LT	0.5 (0.1)	$<10^{-4}$	$>10^4$	0.0885 (0.0010)	1.425 (0.004)	1.216 (0.012)	73	6.0 (0.5)	1.433 (0.004)
YC1.2	2.9 (0.1)	$<10^{-4}$	$>10^4$	0.0851 (0.0064)	1.474 (0.015)	0.388 (0.181)	219	6.2 (0.6)	1.482 (0.015)
YC1.3	8.4 (0.1)	$<10^{-4}$	$>10^4$	0.0807 (0.0046)	1.448 (0.008)	0.276 (0.020)	293	6.0 (0.4)	1.455 (0.008)
YC1.4 [g]	20.1 (0.1)	$<10^{-4}$	$>10^4$	0.1005 (0.0025)	1.431 (0.007)	0.110 (0.049)	917	7.8 (0.2)	1.441 (0.007)
YC1.5	22.6 (0.1)	$<10^{-4}$	$>10^4$	0.0870 (0.0032)	1.398 (0.008)	0.130 (0.020)	669	6.9 (0.3)	1.406 (0.008)
YC1.6	30.6 (0.1)	$<10^{-4}$	$>10^4$	0.0916 (0.0027)	1.459 (0.006)	0.400 (0.014)	229	6.7 (0.3)	1.467 (0.006)
YC001-LB	32.9 (0.1)	$<10^{-4}$	$>10^4$	0.1062 (0.0014)	1.411 (0.003)	0.899 (0.008)	118	7.8 (0.4)	1.420 (0.003)
YC1.7	34.4 (0.1)	$<10^{-4}$	$>10^4$	0.1055 (0.0026)	1.405 (0.007)	0.542 (0.059)	195	8.0 (0.3)	1.414 (0.007)
YC1.8 [g]	35.9 (0.1)	$<10^{-4}$	$>10^4$	0.1316 (0.0012)	1.248 (0.003)	0.610 (0.083)	216	11.6 (0.3)	1.256 (0.003)
PSW1 [h]	n/a	0.70	8.2	0.0470 (0.0031)	1.349 (0.008)	5.752 (0.078)	8	–0.9 (2.5)	1.348 (0.008)

The numbers in parentheses are 95% uncertainties. Isotope data are expressed as activity ratios, the 95% uncertainties for which include allowances for external standard reproducibility and spike calibration uncertainty, although uncertainty in decay constants is not propagated. $[^{230}Th/^{238}U]$ is determined using a mixed spike calibrated against a solution of HU-1, see Hellstrom (2003) for a detailed description of the method and results of standard analyses. Uncorrected age is calculated using the standard U-Th age equation, and employing decay constants of 9.195×10^{-6} and 2.835×10^{-6} for ^{230}Th and ^{234}U, respectively. Corrected age and initial $^{234}U/^{238}U$ activity ratios ($[^{234}/^{238}]i$) have been corrected for detrital Th assuming an initial $^{230}Th/^{232}Th$ activity ratio of 10 ± 5 and propagating its uncertainty via an additional term in the standard U-Th age equation, see Hellstrom (2006) for details. $[^{234}U/^{238}U]i$ is calculated using $[^{234}U/^{238}U]$ and the corrected age.

erosion or non-deposition during the majority of speleothem growth. The exception to this is a singular chalky white horizon near the base of the section which clearly cross-cuts older laminae and is draped by younger laminae (Figure 2). This angular unconformity was created by the break-off of a thin sheet followed by renewed speleothem deposition. Since we are unable to determine when the break-off event occurred or how much material is missing across this unconformity, our interpretations of the speleothem record are restricted to material preserved on either side of the unconformity.

Small (<2 mm) pockets of chalky white calcite are locally present through parts of the speleothem, however there is no evidence of pervasive alteration or diagenesis. The outermost surface of the speleothem is dry and consists of weathered, chalky white calcite, indicating that in the modern environment this speleothem is extinct. Potential sources for carbonate speleothem precipitation in this granitic source terrain include local dissolution of fracture-filling calcite and/or silicate weathering (e.g. Lacelle *et al*., 2007).

Sampling and analytical procedure

Samples were extracted from individual translucent laminations of the flowstone by scratching shallow grooves on a polished section using a stainless steel needle and binocular microscope. Microcrystalline calcite layers were preferentially selected for dating however the scale of laminations prohibited the exclusion of small detrital components. Sample size in each case was less than 0.1 mg and spatial resolution is 0.1 mm. Chemical separation of the U and Th isotopes from the carbonate matrix was not required because of the very high uranium content of the flowstone (not precisely determined, but greater than 100 ppm). Samples were dissolved in 5% nitric acid and a mixed ^{229}Th–^{233}U tracer was added. U/Th isotopic analysis was performed on a Nu Instruments Plasma multi-collector inductively coupled plasma-mass spectrometer (MC-ICPMS) using the method of Hellstrom (2003). After the removal of one outlying analysis, the stratigraphical constraint technique of Hellstrom (2006) indicates the sample to have been deposited with an unusually elevated initial $[^{230}Th/^{232}Th]$, of 12 ± 8, consistent with measured modern $[^{230}Th/^{232}Th]$ of 8.2 in waters of the nearby Paralana Hot Springs, which are similarly fed by local meteoric waters percolating through the Mount Painter Granite (Brugger *et al*., 2005).

Results

Ten U/Th ages were calculated using $[^{230}Th/^{232}Th]_i$ of 10 ± 5, imparting age uncertainties of up to ± 1.0 ka (Figure 2C; Table 1). The speleothem contains little detrital Th and yields a series of ages ranging from 11.6±0.3 ka from the innermost lamination adjacent to the cave wall to 5.2±1.0 ka from the outermost lamination, indicating speleothem growth in the latest Pleistocene and early to middle Holocene. Speleothem thickness measurements between successive ages were used to generate an age versus growth rate plot (Figure 2D). The earliest detected growth at *c*. 11.6 ka is confined to the ~0.3 mm thick layer at one corner of the section beneath the unconformity. The lamination immediately overlying the unconformity yields an age of *c*. 8.0 ka. Because we do not know the growth history of the speleothem from *c*. 11.6 to 8.0 ka, or prior to 11.6 ka, our interpretations are restricted to ~11.6 ka and 8.0 ka to present. The next part of the lamination sequence overlying the *c*. 8 ka site yields an age of *c*. 7.8 ka that is within analytical error of the *c*. 8 ka age. This is separated from the next U/Th age of *c*. 6.7 ka by a series of thin laminations with no apparent unconformities spanning a sample width of ~2.3 mm, implying relatively slow but continuous growth during the *c*. 7.8–6.7 ka interval. The next age of 6.9 ± 0.3 ka is within analytical error of the 6.7 ka age and situated ~8 mm from this site, implying an increase in speleothem growth rate beginning at *c*. 6.7–6.9 ka. The overlying age of *c*. 7.8 ka is anomalous and the only age we obtained that does not conform to the stratigraphic age pattern. We suspect that during deposition of this part of the sample, either $[^{230}Th/^{232}Th]_i$ became very high for a while (possible, as very high $[^{230}Th/^{232}Th]_i$ samples often have high $[^{230}Th/^{232}Th]_i$ variability), or the system was somehow not closed since deposition (unlikely, as the sample is composed of sound calcite). The next three U/Th ages of *c*. 6.0–6.2 ka are within analytical error and span a width of ~8 mm, implying the period of relatively 'rapid' speleothem growth

continued to *c*. 6 ka. The outermost lamination is ~0.4 mm from the outermost *c*. 6 ka site and yields an age of 5.2±1.0 ka, suggesting a slowing of speleothem growth from *c*. 6 to 5 ka and termination of growth by *c*. 5 ka. Although speleothem growth from *c*. 8 to 5 ka was likely episodic on timescales finer than the resolution of U-Th age dating as indicated by the presence of hundreds of laminations, the absence of discernable unconformities during this time interval implies no major interruptions in mid-Holocene growth. The age–growth rate plot reveals speleothem growth at rates of 2–4 mm/kyr from *c*. 8 to 7 ka, a marked increase to rates of 10–20 mm/kyr at *c*. 7–6 ka, a decrease to rates of 0.2–0.4 mm/kyr at *c*. 6–5 ka and a cessation of growth at *c*. 5 ka. Providing speleothem ages provide a proxy for local climate conditions, our results suggest more a more effectively humid climate at *c*. 12–11 ka and *c*. 8–5 ka marked by a peak in humidity between 7 and 6 ka, followed by the onset of effectively arid conditions similar to present at 5–4 ka. It is highly likely that the moisture required to sustain the rapid *c*. 7–6 ka growth rates would have been enough to sustain perennial stream flow in Yudnamutana Creek. It is inconceivable that one river system in the range could be hydrologically active for at least 2000 years without at the very least reflecting a regional *in situ* precipitation signal. This is explored in more detail in the Discussion.

Stable isotopic analysis of the Yudnamutana speleothem

Sampling and analytical procedure

Thirty-eight carbonate sample powders were milled at ~1 mm intervals across the growth axis of the Yudnamutana speleothem for stable oxygen and carbon isotopic analysis. Milling was performed using a 400 µm diamond drill bit installed in a vertically mounted Dremel tool. Each sample represents a mixture of several (*c*. 2–10) individual carbonate laminations. $\delta^{18}O$ and $\delta^{13}C$ values were determined using an automated ThemoFinnigan GasBench II connected under continuous helium flow conditions to a ThermoFinnigan Delta V Plus isotope ratio mass spectrometer. For individual samples, approximately 300 µg of sample powder was placed in a sealed 12 ml exetainer vial and flushed with ultra-high purity helium for 10 min. Liquid orthophosphoric acid was then added to the vial and allowed to react with the sample carbonate at 72°C for 1 h. Carbon dioxide produced by the acid-carbonate reaction was then injected into a PoraPlot Q gas chromatography capillary column and analyzed for stable carbon and oxygen isotopic compositions. Ten sample gas injection $\delta^{18}O$ and $\delta^{13}C$ values were corrected for linearity and normalized to the V-PDB scale based on replicate analyses of certified reference carbonate materials, NBS-19 ($\delta^{18}O$= −2.20‰ V-PDB; $\delta^{13}C$ = 1.95‰ V-PBD) and NBS-18 ($\delta^{18}O$= −23.00‰ V-PDB; $\delta^{13}C$ = −5.01‰ V-PBD). Sample $\delta^{18}O$ and $\delta^{13}C$ values are accurate to ±0.2‰ V-PDB based on analysis of certified reference materials (NBS-18, NBS-19), an internal lab standard (MERCK carbonate), and replicate analysis of individual samples. Analytical precision is better than 0.1‰ V-PDB for both $\delta^{18}O$ and $\delta^{13}C$ values based on standard on–off tests performed on ultra-high purity carbon dioxide reference gas at the start of each analytical sequence. A linearity correction factor was also determined prior to each analytical sequence for both $\delta^{18}O$ and $\delta^{13}C$ values.

Table 2. Stable isotopic results for the Yudnamutana speleothem

Distance from edge (mm)	$\delta^{13}C$ (‰ V-PDB)	$\delta^{18}O$ (‰ V-PDB)
0	−9.67	−5.11
1	−8.8	−4.37
2	−10.91	−5.23
3	−9.22	−4.18
4	−11.16	−5.48
5	−11.78	−5.67
6	−11.5	−5.38
7	−11.56	−5.33
8	−10.47	−5
9	−10.72	−5.37
10	−11.14	−5.45
11	−9.97	−4.47
12	−10.54	−5.08
13	−10.15	−5.23
14	−9.32	−4
15	−9.39	−4.42
16	−10.65	−5.11
17	−10.32	−5.41
18	−8.49	−4.16
19	−10.93	−5.61
20	−9.69	−4.61
21	−9	−4.2
22	−8.2	−3.46
23	−9.65	−4.24
24	−9.56	−4.32
25	−9.46	−4.74
26	−10.07	−5.33
27	−9.86	−4.9
28	−9.64	−4.98
29	−10.51	−5.24
30	−9.94	−4.85
31	−9.27	−4.68
32	−8.59	−4.27
33	−9.21	−4.41
34	−9.24	−4.71
35	−9.72	−4.5
36	−7.71	−3.66
37	−6.04	−2.81

Results

The oxygen and carbon isotopic composition of the Yudnamutana speleothem exhibits marked variability and distinct trends (Table 2, Figure 3). $\delta^{18}O$ values range between −2.7‰ and −5.7‰ (V-PDB) with a mean value of −4.7‰ and standard deviation of 0.7‰. $\delta^{13}C$ values range between −11.8‰ and −6.0‰ (V-PDB) with a mean value of −9.8‰ and standard deviation of 1.1‰. There is an overall decrease in both $\delta^{18}O$ and $\delta^{13}C$ values with decreasing age. However, the most salient characteristics of the stable isotopic data are: (1) strong positive covariance between $\delta^{18}O$ and $\delta^{13}C$ values (Figure 4); (2) five ≥+1.0‰ excursions in both $\delta^{18}O$ and $\delta^{13}C$ values between 6 and 7 ka (Figure 3).

Strong positive covariance between $\delta^{18}O$ and $\delta^{13}C$ values along the growth axis (i.e. across carbonate laminae) of a speleothem can result from a variety of processes. The most likely mechanism of such positive co-variation is kinetic fractionation associated with isotopic Rayleigh distillation of drip water DIC and incomplete oxygen isotope equilibration between isotopically evolved DIC and water (Mickler *et al*., 2006). Alternative environmental drivers are also possible, including: monsoonal/tropical amount effects, temperature effects, changes in hydrologic balance, and establishment of dry-summer wet-winter climate regimes (Lachniet, 2009; Mickler *et al*., 2006). The 38 carbonate samples analyzed here exhibit a strong positive covariance (r^2 = 0.85) across the whole of the speleothem growth period

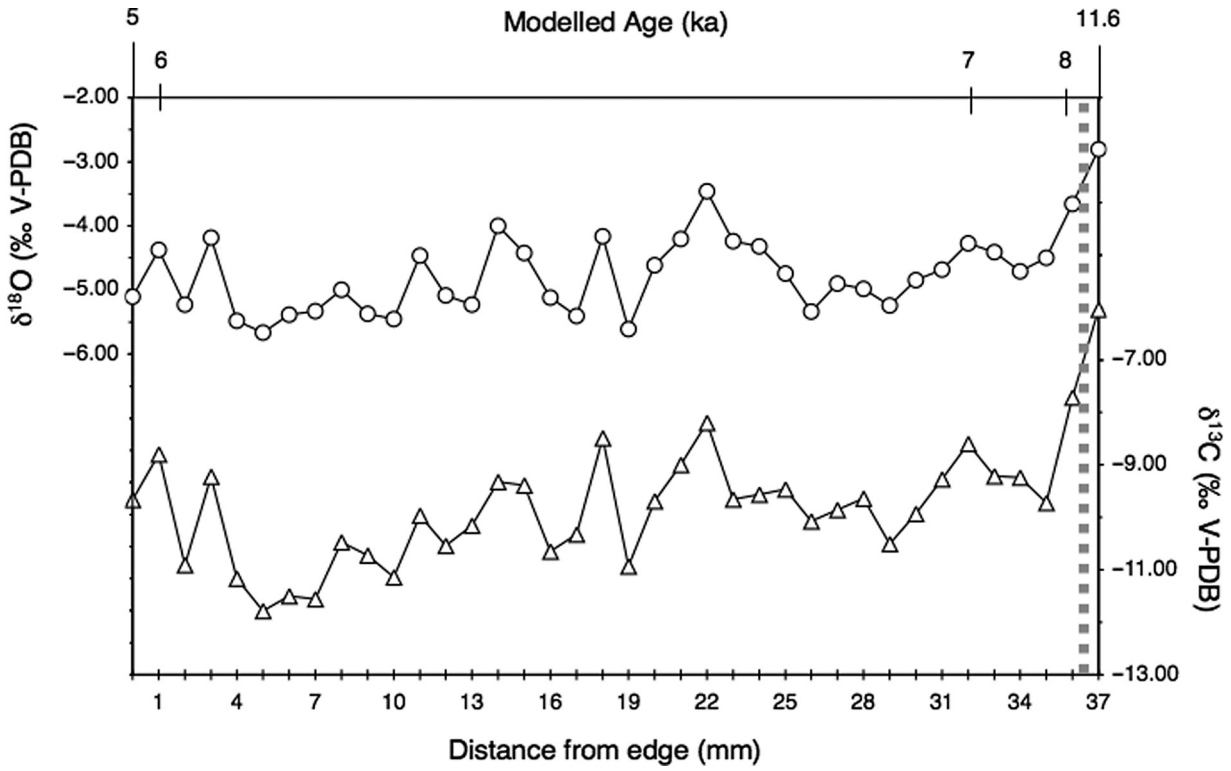

Figure 3. $\delta^{18}O$ (circles) and $\delta^{13}C$ (triangles) data for the Flinders Ranges speleothem plotted against sample depth (i.e. distance from edge). Approximate age constraints based on U-Th age model presented in Figure 2. Isotopic analysis was performed on carbonate powders milled from 1 mm wide swaths along the speleothems growth axis. Dashed grey line indicates location of a clear depositional hiatus (i.e. unconformity) in speleothems growth

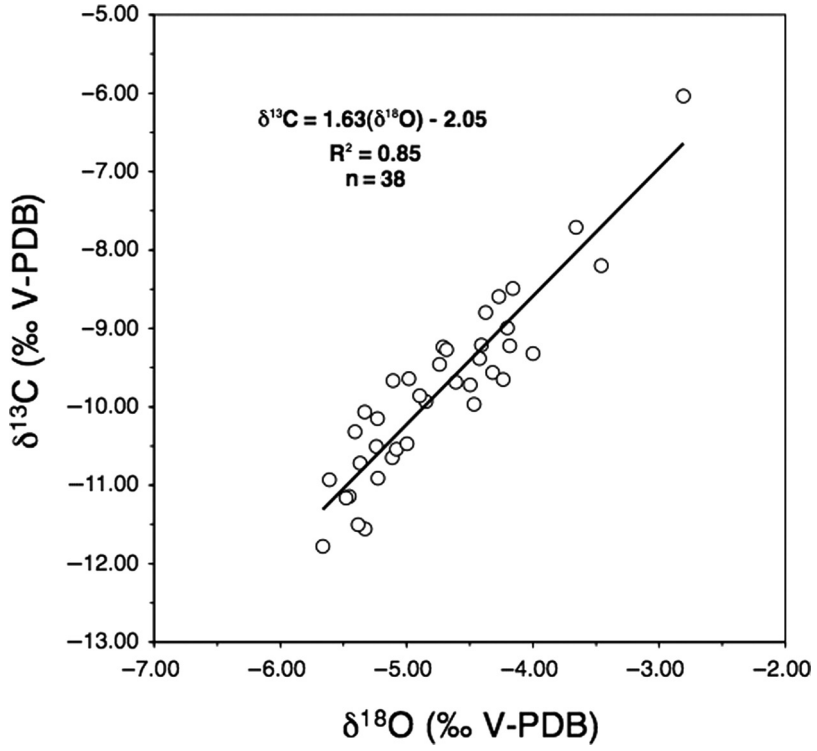

Figure 4. $\delta^{13}C$ versus $\delta^{18}O$ scatter-plot for all 38 carbonate powders analysed. Line equation and correlation coefficient, R^2, are based on simple least-squares linear regression of the data shown

suggesting that the mechanism of this covariance must also explain the observed positive excursions in carbonate isotopic compositions through time.

Five distinct isotopic excursions, towards more positive δ-values, are recognized in the Yudnamutana speleothem during the period of rapid growth (~6–7 ka). It is unlikely that changes in

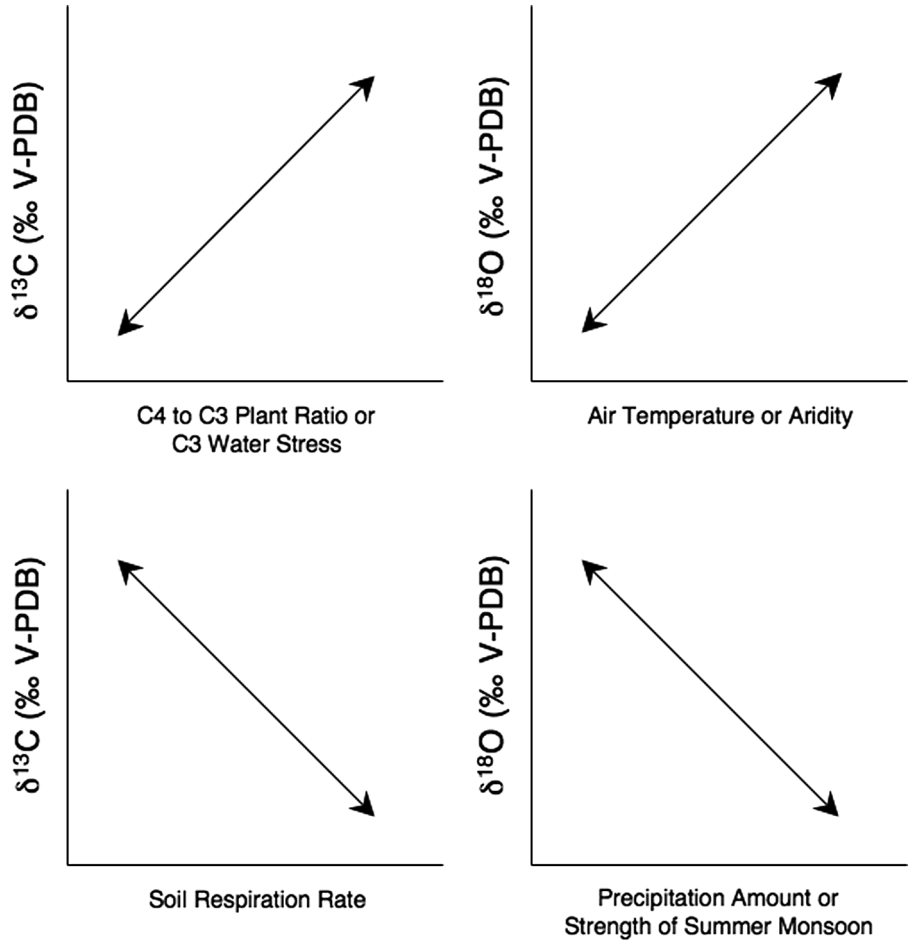

Figure 5. Schematic representations of the effects of various environmental factors on speleothem $\delta^{13}C$ and $\delta^{18}O$ values (based on Mickler *et al*., 2006). Combinations of environmental effects with similar direction carbon and oxygen isotopic effects (e.g. increased C4 to C3 plant ratio and increased aridity, or decreased soil respiration rate and decreased summer monsoon intensity) will produce positive covariance between speleothem $\delta^{13}C$ and $\delta^{18}O$ values. Combinations of environmental effects with opposite direction carbon and oxygen isotopic shifts will produce negative covariance between speleothems $\delta^{13}C$ and $\delta^{18}O$ values

the temperature of carbonate formation (under isotopic equilibrium conditions) was a primary driver for these excursions as temperature decreases between 5° and 10°C are required to produce +1.0 to +2.0‰ shifts in calcite $\delta^{18}O$ values, based on the equilibrium fraction equation of Kim and O'Neil (1997) and assuming the oxygen isotope composition of drip waters remained a constant −5.0‰ (V-SMOW). International Atomic Energy Agency (IAEA) modeling indicates that modern precipitation $\delta^{18}O$ values in the northern Flinders Range are expected to range between −4 and −6‰ V-SMOW (IAEA, 2001), and a recent study in the Mount Lofty Ranges, immediately to the south of the Flinders Ranges, indicates meteoric waters in the region vary between −4.4 and −5.9‰ V-SMOW (Guan *et al*., 2009).

The required extreme shifts towards markedly colder conditions, and the strong indication that non-equilibrium isotopic fractionations occurred throughout the speleothem growth interval, indicate temperature effects played a relatively minor role in determining the isotopic composition of the Yudnamutana speleothem. Rather, these excursions likely represent non-equilibrium isotopic effects associated with episodic perturbations to the local carbon and hydrologic cycles. Excess CO_2 is dissolved in shallow subsurface waters during periods of heightened aridity (i.e. evaporative enrichment) or increased soil respiration associated with relatively wetter conditions, and changes in the pCO_2 gradient between drip waters and the cave atmosphere will influence the extent of non-equilibirum fractionation effects between drip water DIC and carbonate precipitates. The positive isotopic covariance and isotopic excursions recognized in the Yudnamutana speleothem may result from the combined effects of increased soil respiration during a period (~8 to 5 ka) of relatively high precipitation (i.e. shift towards more negative $\delta^{18}O$ and $\delta^{13}C$ values; Figure 5) and shorter-lived episodes of heightened aridity accompanied by decreased soil respiration rates and increased water stress on C_3 woodland plants (i.e. shift towards more positive $\delta^{18}O$ and $\delta^{13}C$ values; Figure 5). This interpretation agrees well with other climatic and environmental proxies suggesting south-central Australia was relatively wet with more abundant woodlands in the early to middle Holocene (McCarthy and Head, 2001; Singh and Luly, 1991). However, alternative explanations (i.e. simple kinetic fractionation in the absence of an environmental driver) cannot be ruled out.

Holocene super-flood record from Wilkatana alluvial fans

Mapping, OSL and ^{14}C dating of coarse-grained cut-and-fill alluvial sequences deposited in the fanhead trench of the North Wilkatana fan were used to develop proxy data for the age and recurrence of large magnitude floods in the Holocene (Quigley *et al*., 2007a).

Transported boulders with diameters up to 80 cm are present within these alluvial gravels, indicating deposition occurred during extremely large stream discharge events or 'super-floods'. Deposition ages derived from alluvium in these cut-and-fill terraces decrease with decreasing terrace height above the modern stream, from 29 ± 2 ka (T_7), 5.9 ± 0.1 ka (T_5), 4.2 ± 0.6 ka (T_4), 3.1 ± 0.2 ka (T_3) to 1.8 ± 0.1 ka (T_2), with at least one undated event (T_6) between *c*. 29 ka and *c*. 5.9 ka and one event (T_1) between *c*. 1.8 ka (T_2) and present (Quigley *et al*., 2007a; Williams *et al*., 1973). The South Australian flood data base (McCarthy *et al*., 2006) provides historical records of two large regional rainfall events (18 July 1916 and 9 December 1886) for which flooding was recorded in Mt Arden Creek, which has a catchment that shares a drainage divide with the North Wilkatana catchment, located ~3.5 km east of the North Wilkatana alluvial fan site. It is therefore conceivable that one of these events may have been associated with the formation of the T_1 terrace, although no historical records from North Wilkatana Creek are available. An intact fence constructed across the T_1 terrace and active stream channel in the 1950s (A. Smart, personal communication, 2004) constrains the age of T_1 to ≥1950.

Collectively, the terrace depositional ages indicate at least five large flood events occurred between *c*. 5.9 ka and 1950 (recurrence interval ~1200 ± 250 yr), while at least three flood events occurred at *c*. 29–5.9 ka (recurrence interval ~7700 ± 700 yr), assuming all large floods produced aggradational terraces and all aggradational terraces were preserved and identified. The presence of only one aggradational terrace between *c*. 29 and 6 ka is interpreted to indicate either (1) a scarcity of high discharge flood events over this interval or (2) removal of paleoflood deposits by younger flood events. We cannot dismiss the latter hypothesis outright, and leave open the possibility that this flood record is somewhat fragmentary. However, several regional observations suggest that the large flood frequency was reduced in the Late Pleistocene relative to the Holocene. First, there is a paucity of coarse-grained alluvial deposits of *c*. 29–6 ka age throughout the region, suggesting that the record captured by the study site is not unique to this location (Quigley *et al*., 2007 a; Williams, 1973; Williams *et al.*, 2001). Second, sequences of fine-grained, aeolian sediment-derived deposits up to ~18 m thick aggraded within Flinders Ranges catchments ~ 120 km north of the Wilkatana site between ~30 and 16 ka, which Williams *et al*. (2001) interpreted to mark a reduced occurrence or absence of extreme flood events during the Late Pleistocene because of weakened incursion of summer rainfall from northern Australia. Third, the near total absence of C_4 plants in the Lake Eyre inferred from carbon isotopes in fossil emu eggshells led Johnson *et al*. (1999) to interpret the *c*. 28 and 15 ka interval as a time of reduced temperatures, reduced summer rainfall and reduced rainfall variability associated with decreased effectiveness of the ASM. A reduction in ASM activity may have been associated with lower LGM sea-levels and/or a more northerly position of the subtropical ridge (Hesse *et al*., 2004), which would have limited the southward penetration of tropical storms into the arid continental interior.

Discussion

Summary of speleothem and alluvial records

Thin section observation and U-Th dating reveals that the Yudanamutana speleothem was deposited at *c*. 11 ka and between *c*. 8 and 5 ka, with most rapid depositional rates at *c*. 7–6 ka. In the modern climate, this cave is dry with no active speleothem growth, hence we interpret these results to indicate increased EP at the study site relative to present during the early middle-Holocene 'climatic optimum'. During this time, it is likely that EP was high enough to sustain perennial stream flow in the adjacent, presently ephemeral stream system, implying a natural environment drastically different from present. The *c*. 5 ka onset of modern arid conditions is interpreted as the time at which deposition ended in this speleothem, as it is situated in an ideal location to capture any water infiltrating into this cave. C and O isotopic covariance and excursions recognized within the speleothem record are interpreted to reflect isotopic effects associated with variable drip water CO_2 degassing rates associated with climatically induced changes in the degree of plant respiration and soil moisture. The increase in isotopic variance between 7 and 6 ka suggests that this 1000 yr interval was associated with increased EP variability relative to the bounding intervals, in addition to increased overall EP.

The chronology of cut-and-fill aggradational terraces in the Wilkatana area is interpreted to mark an increased frequency of extreme rainfall events and associated floods in the Holocene relative to the Late Pleistocene, an interpretation consistent with other proxy data from this region. We cannot state absolutely when this change occurred, however, we note that at least five flood-related alluvial terraces have been deposited in the last *c*. 6 kyr, in contrast with the deposition of only three such terraces between *c*. 29 and *c*. 6 kyr.

Correlations with other climate proxy data

Interpretations of paleovegetation records derived from fossil pollen and plant macrofossils in Holocene stick-nest rat middens in the Flinders Ranges indicate a dominance of woodland and shrubland communities with herbaceous understoreys in the northern ranges and shrublands with an understorey of herbaceous taxa and chenopods in the central ranges at 7–5 ka (McCarthy and Head, 2001) and possibly as early as *c*. 9 ka (McCarthy *et al*., 1996). These data suggest warmer, wetter and more homogeneous climatic conditions than present from *c*. 7 to 5 ka. Singh and Luly (1991) found that abundances of chenopod shrublands and ephemeral daisies decreased and grasses (associated with high summer rainfall) increased between *c*. 13 and 4.4 ka, interpreted to indicate a decrease in winter precipitation and increase of summer precipitation associated with strengthening of the ASM. From *c*. 4 to 2 ka, shrubland communities declined in the central ranges to be replaced by chenopod shrublands with a less diverse component of herbaceous taxa in the understorey, interpreted to indicate increased climatic aridity and variability (McCarthy and Head, 2001; Singh and Luly, 1991). The increase in chenopod shrublands and ephemeral asteraceous vegetation after *c*. 4 ka was interpreted by Singh and Luly (1991) to indicate declining summer precipitation associated with a deterioration of the ASM. The timing of shifts in paleovegetation throughout the northern and central Flinders Ranges, interpreted to mark climate-related increases in EP at *c*. 7–5 ka and decreased EP since *c*. 4–5 ka, is remarkably consistent with the timing of EP changes inferred from the Yudnamutana speleothem data, implying that the latter provides a robust proxy for regional climate change.

Stratigraphic evidence from playa lakes provides larger-scale, integrated records of EP changes. Lake Eyre experienced a perennial

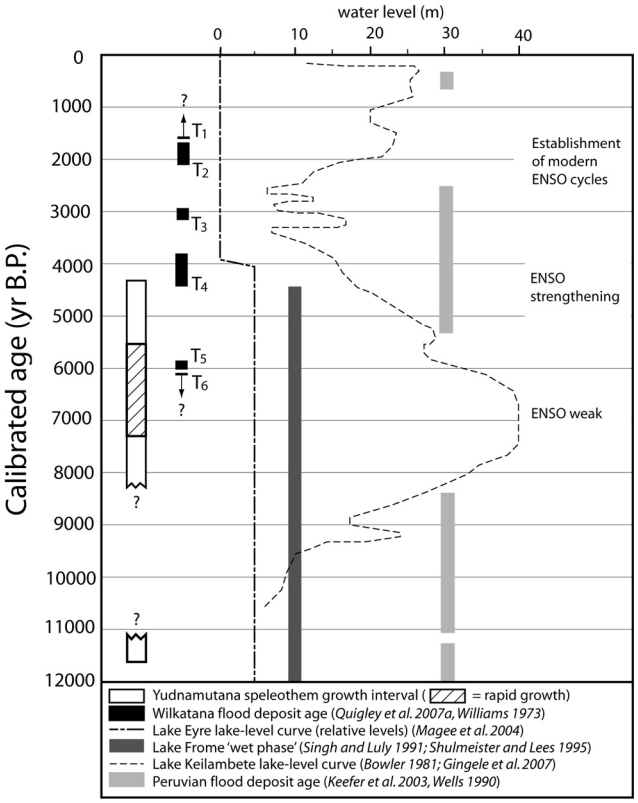

Figure 6. Correlative plot of various climate proxies, paleoclimatic interpretations and inferred temporal variability in ENSO intensity. Jagged bar ends and question marks on speleothem age range between *c.* 8 and 11 ka denote the time interval for which speleothem growth history is unknown because of the presence of an unconformity spanning this interval. Plotted age range of speleothem and flood deposits include age errors. Lake Eyre lake-level curve calibrated to show relative deviation from a modern lake level value of 0. Peruvian flood deposit ages interpreted as ENSO proxies by Keefer *et al.* (2003). ENSO behavior inferred from presented data and other data sets described in text. The Yudnamutana speleothem and Wilkatana alluvial records are consistent with a shift from weakened ENSO activity at *c.* 8–5 ka to stronger ENSO intensity from *c.* 5 ka to present

lacustrine phase from *c.* 12 ka to *c.* 4 ka, interpreted to reflect increased ASM activity, followed by drying and establishment of the modern ephemerally flooded playa regime (Gillespie *et al.*, 1991; Magee *et al.*, 2004). The absence of early- to mid-Holocene beaches imply that *c.* 12–4 ka perennial lake levels were below the highest floods of the modern ephemeral regime, suggesting a change to less frequent but more extreme rainfall events in the source catchment after *c.* 4 ka (Magee *et al.*, 2004). Since the Lake Eyre catchment area is situated within the modern ASM rainfall zone (Figure 1), lake paleohydrology relates to EP changes in northern and central Australia, as opposed to local changes in EP as recorded by the speleothem and alluvial deposits. However, the general consistency in timing and interpretations of these records confirms that the EP was elevated relative to present in the early middle-Holocene EP, and that EP was reduced and large flood frequency was increased over large parts of the Australian continent by *c.* 5–4 ka.

A variety of other climate proxies from across Australia provide evidence for increased EP during the early middle-Holocene climatic optimum (Figure 6). Pollen records from coastal regions of eastern and northern Australia, where ENSO exerts strong influence on modern climate (Nicholls, 1992), show significant increases in EP from *c.* 8 to 4 ka (McGlone *et al.*, 1992; Shulmeister and Lees, 1995). Holocene sedimentary records from Lake Keilambete (Figure 6) (Bowler, 1981; Chivas *et al.*, 1986, 1993; De Deckker, 1982) and Blue Lake in southeast Australia (Stanley and De Deckker, 2002) indicate low lake levels prior to *c.* 8 ka, high lake levels from *c.* 8 to 4.5 ka, low but highly variable levels from *c.* 4.5 to 2 ka, and moderate levels over the past 2 kyr, with a distinct drop in levels over the past several hundred years (Bowler, 1981). $^{87}Sr/^{86}Sr$ and $^{144}Nd/^{143}Nd$ ratios and clay contents of Murray Basin sediment deposited offshore in the Murray River mouth (Figure 1) suggest fluvial pulses at *c.* 13.5–11.5 ka and *c.* 9.5–7.5 ka, interpreted to indicate a more humid climate, transitional conditions at *c.* 9.5–11.5 ka and *c.* 7.5–5 ka, and enhanced dust signatures associated with arid conditions from *c.* 5 ka to the present (Gingele *et al.*, 2007). Pollen records (Markgraf *et al.*, 1986), lake levels (Harrison, 1993), and speleothem data (Xia *et al.*, 2001) from Tasmania indicate increased EP in the middle Holocene, particularly at *c.* 7 ka. The wide variety and broad spatial extent of evidence for increased EP in the mid Holocene, followed by increased aridity and climate variability at *c.* 5 ka, suggests that the EP changes recorded by the Yudnamutana speleothem were continental in scale, occurring in the tropics, temperate regions, and arid interior of the Australian continent.

Origin of the middle-Holocene 'climatic optimum' in southern Australia

Contemporary annual rainfall variability in the study region is modulated by complex interactions amongst broad-scale atmospheric arrangements (SO, ASM, SAM) associated with sea surface temperature gradients in the Pacific, Indian, and Southern Oceans (Evans *et al.*, 2009; Meneghini *et al.*, 2007) and influenced by local topography. In general, lower (higher) than average annual rainfall is observed during periods of warming (cooling) in the central and east Pacific and cooling (warming) in the west Pacific associated with El Niño (La Niña) conditions. Anomalously cool (warm) waters in the northeast Indian Ocean and warm (cool) waters in the west Indian Ocean associated with positive (negative) phases of the IOD, together with warmer (cooler) than usual waters in the *southeast* Indian Ocean are associated with lower (higher) than average rainfall in the study region (Ashok *et al.*, 2003; Evans *et al.*, 2009). Although the speleothem site lies south of the ~25°S boundary typically regarded as the southern limit of ASM-dominated precipitation (Suppiah, 1992), the tendency towards summer precipitation in this region suggests that southward incursions of ASM-related rainfall do in fact reach this area. The positive (negative) phase of SAM is associated with a southward (northward) migration of the polar front jet, and a weakening (strengthening) of westerly winds between ~30 and 45°S, resulting in lower (higher) than average winter precipitation across southern Australia, including the study region (Meneghini *et al.*, 2007). The inter-relationships amongst these climate modes are complex and the focus of many studies (e.g. Ashok *et al.*, 2003; Evans *et al.*, 2009; Ummenhofer *et al.*, 2009), however several authors have proposed teleconnections amongst the IOD, ASM, ENSO, and SAM (e.g. Behera *et al.*, 2006; Carvalho *et al.*, 2005; England *et al.*, 2006; L'Heureux and Thompson, 2006; Semenov *et al.*, 2008; Suppiah, 1992; Wright, 1997). For example, Semenov *et al.* (2008) used composite atmospheric circulation models to demonstrate that during La Niña ascending motions in the region of the

ASM are subject to abrupt intensification, leading to a maximum displacement of ASM-related rains deep into the Australian continent. Carvalho *et al*. (2005) describe a tendency for the positive (negative) phase of SAM to occur during La Niña (El Niño) events.

The early to middle Holocene was an interval of decreased ENSO activity, characterized by infrequent or absent El Niños (Figure 6) (e.g. Gagan *et al*., 1998; Gomez *et al*., 2004; Liu *et al*., 2000; McGlone *et al*., 1992; Rodbell *et al*., 1999; Sandweiss *et al*., 1996; Shulmeister and Lees, 1995; Tudhope *et al*., 2001) and prevalence of a La Niña-like mean climatic state in the tropical Pacific Ocean (Koutavas *et al*., 2002). The scarcity of El Niño-related droughts, sustenance of a mean La Niña climatic state, and increase in ASM intensity (Shulmeister and Lees, 1995) would have created an environment favoring higher-than-present summer EP in Australia's arid interior (Singh and Luly, 1991; McCarthy and Head, 2001; Magee *et al*., 2004). Although the stable isotopic data from the Yudanamutana speleothem does not allow us to discriminate between northerly (Indian Ocean, ASM) and southerly (Southern Ocean) sources for precipitation, the dominance of summer rainfall-related northern taxa over winter rainfall-related southern taxa in the *c*. 13–4.5 ka Lake Frome record (Singh and Luly, 1991) supports our hypothesis of a southward expansion of the ASM-related summer rainfall zone to beyond 30°S, and associated increase in EP at higher latitudes, during the Holocene climatic optimum.

A more active early middle-Holocene ASM implies that the ITCZ would have been shifted further south at this time (Shulmeister and Lees, 1995). This was likely accompanied by a southward shift of the polar frontal jet (PFJ), historically linked to the positive SAM phase that causes drier winters in southern Australia due to the inability for rain-bearing fronts to reach lower latitudes (Hendon *et al*., 2007; Meneghini *et al*., 2007). On the basis of a southern Australian source region for dust deposition in New Zealand, Marx *et al*. (2009) inferred that southern Australia was 'dry' during the early middle Holocene (*c*. 7.8–4.8 ka) because of a southward shift in the ITCZ. However this is at odds with the Yudanamutana speleothem record and the other paleo-environmental records from southeast Australia discussed above (Bowler, 1981; De Deckker, 1982; Harrison, 1993; Stanley and De Deckker, 2002). We reconcile these relationships by suggesting that while the La Niña-like climatic state increased the amount of atmospheric moisture available for precipitation, fluctuations in the position of the ITCZ and position and strength of the westerly PFJ related to SAM variability impacted on the location and magnitude of precipitation across southern Australia (e.g. Hill *et al*., 2009; Meneghini *et al*., 2007). Maximum southern extents of these systems (positive SAM) would have resulted in wetter summers and drier winters in the study area, accounting for the paleovegetation records and, potentially, the observed increase in speleothem isotopic variance during times of EP maxima (*c*. 7–6 ka). Further to the south in northern Tasmania, where modern rainfall variability is strongly linked to ENSO and SAM (Hill *et al*., 2009), frequent changes in speleothem growth rate are associated with seven different short-duration (≤600 yr) climate stages between *c*. 9.2 and 5.1 ka (Xia *et al*., 2001). This variance provides evidence for the early middle-Holocene oscillations in the position and strength of the westerlies we propose. While such oscillations appear not to have been of sufficient magnitude and/or duration to leave a distinct signal in paleolake levels, frequent SAM-related changes between wetter (windier) and drier (less windy) conditions provide a feasible mechanism for generating dust across southern Australian (Marx *et al*., 2009) despite a climatic regime generally characterized by higher-than-present EP.

The onset of the 'modern' climatic regime: Implications for contemporary climate change and climate-weather interactions

After *c*. 5 ka, changes in ENSO dynamics, including the more frequent occurrence of El Niños, are likely have impacted on the other climate modes that deliver rainfall to southern Australia. These impacts would have included a reduced strength of the ASM, decreasing the amount of summer rainfall delivered to the Yudnamutana site, which coupled with El Niño-triggered droughts, resulted in significant EP reduction and termination of speleothem growth. The influence of SAM activity on southern Australian rainfall is likely to have increased as the position of moisture-bearing westerly winds shifted northward, bringing increased winter rainfall. However, these shifts contribute little overall rainfall to the Yudnamutana site, which remains in a weakly summer-dominated rainfall zone. The climate changes across the Australian continent over the last *c*. 5–4 kyr are, in general, of lower magnitude that the climate changes accompanying the demise of the early middle-Holocene climatic optimum at *c*. 5–4 kyr. We thus attribute the onset of the 'modern' climatic regime to the *c*. 5–4 kyr interval.

The timing and origin of the increased large flood frequency in the Wilkatana area, and possibly the broader region, remains a motivation for future research. It is possible that the transition to a more arid environment after *c*. 5 ka resulted in decreased vegetative cover and increased runoff, allowing for extreme rainfall events to leave a stronger sedimentological imprint on the landscape. In this sense, there may be a generalized linkage amongst ENSO activity and flooding in south-central Australia. The La Niña years of 1886, 1916, 1917, 1950, 1954–1956, and 1973–1975 were accompanied by some of the largest and most widespread flooding in Australia's history, including flooding near the Wilkatana study site in 1886 and 1916 (http://www.bom.gov.au/lam/climate/levelthree/c20thc/flood.htm). However, the *c*. 5 ka transition to more arid climates might also have increased the frequency and magnitude of extreme rainfall events. Using climate simulation models, McInnes *et al*. (2003) documented an increase in extreme rainfall events over much of South Australia despite decreases in average rainfall, implying that storms may become more intense even in a climate that becomes drier on average. Turcotte and Greene (1993) showed that the ratio of large flood to small flood frequency in the continental USA increases with increasing climatic aridity. In this context, as southern Australia descends further into aridity, our chronology of paleoflood events may provide a context for investigating the relationships amongst extreme rainfall events and anthropogenically influenced climate change.

Acknowledgments

We thank Martin Williams and Gerald Nanson for providing thorough and encouraging reviews that helped improve the manuscript.

References

Abram NJ, Gagan MK, Liu Z, Hantoro WS, McCulloch MT and Suwardadi BW (2007) Seasonal characteristics of the Indian Ocean Dipole during the Holocene epoch. *Nature* 445: 299–302.

Allan RJ (1985) *The Australasian Summer Monsoon, Teleconnections, and Flooding in the Lake Eyre Basin*. South Australian Geographical Papers, no. 2, Royal Geographical Society of Australasia, 47 pp.

Ashok K, Guan Z and Yamagata T (2003) Influence of the Indian Ocean dipole on the Australian winter rainfall. *Geophysical Reseach Letters* 30: doi:10.1029/2003GL017926.

Asmerom Y, Polyak V, Burns S and Rassmussen J (2007) Solar forcing of Holocene climate: New insights from a speleothem record, southwestern United States. *Geology* 35: 1–4.

Behera SK, Luo J-J, Masson S, Rao SA, Sakuma H and Yamagata T (2006) A CGCM study on the interaction between IOD and ENSO. *Journal of Climatology* 19: 1688–1705.

Bond G, Showers W, Cheseby M, Lotti R, Almasi P, deMenocal P *et al.* (1997) A pervasive millennial-scale cycle in North Atlantic Holocene and Glacial climates. *Science* 278: 1257–1266.

Bowler JM (1981) Australian salt lakes: A palaeohydrologic approach. *Hydrobiologia* 82: 431–444.

Brugger J, Long N, McPhail DC and Plimer I (2005) An active amagmatic hydrothermal system: The Paralana hot springs, Northern Flinders Ranges, South Australia. *Chemical Geology* 222: 35–64.

Carvalho LMV, Jones C and Ambrizzi T (2005) Opposite phases of the Antarctic Oscillation and relationships with intraseasonal to interannual activity in the tropics during the Austral summer. *Journal of Climate* 18: 702–718.

Chivas AR, De Deckker P and Shelley JMG (1986) Magnesium content of non-marine ostracods: A new palaeosalinometer and palaeothermometer. *Palaeogeography, Palaeoclimatology, Palaeoecology* 54: 43–61.

Chivas AR, De Deckker P, Cali JA, Chapman A, Kiss E and Shelley JMG (1993) Coupled stable-isotope and trace-element measurements of lacustrine carbonates as paleoclimatic indicators. In: Swart PK, Lohmann KC, McKenzie JA and Savin SM (eds) *Climate Change in Continental Isotopic Records*. America Geophysical Union, Geophysical Monograph 78: 113–121.

Coats RP (compiler) (1973) *Copley, South Australia*. Geological Survey of South Australia, Geological Series Explanatory Notes, Sheet SH/ 54–9.

Cupper ML (2005) Last glacial to Holocene evolution of semi-arid rangelands in southeastern Australia. *The Holocene* 15: 541–553.

De Deckker P (1982) Holocene ostracodes, other invertebrates and fish remains from cores of four maar lakes in southeastern Australia. *Proceedings Royal Society Victoria* 94: 183–219.

Drysdale RN, Zanchetta G, Hellstrom JC, Maas R, Fallick AE, Pickett M *et al.* (2006) Late Holocene drought responsible for the collapse of Old World civilizations is recorded in an Italian cave flowstone. *Geology* 34: 101–104.

Drysdale R, Zanchetta G, Hellstrom J, Fallick A, McDonald J and Cartwright I (2007) Stalagmite evidence for the precise timing of North Atlantic cold events during the early last glacial. *Geology* 35: 77–80.

England MH, Ummenhofer CC and Santoso A (2006) Interannual rainfall extremes over southwest Western Australia linked to Indian Ocean climate variability. *Journal of Climate* 19: 1948–1969.

Evans AD, Bennett JM and Ewenz CM (2009) South Australian rainfall variability and climate extremes. *Climate Dynamics* 33: 477–493.

Gagan M, Ayliffe L, Hopley D, Cali J, Mortimer G, Chappell J *et al.* (1998) Temperature and surface-ocean water balance of the mid-Holocene tropical western Pacific. *Science* 279: 1014–1018.

Gillespie R, Magee JW, Luly JG, Dlugokencky E, Sparks RJ and Wallace G (1991) AMS radiocarbon dating in the study of arid environments: Examples from Lake Eyre, South Australia. *Palaeogeography, Palaeoclimatology, Palaeoecology* 84: 333–338.

Gingele F, De Deckker P and Norman M (2007) Late Pleistocene and Holocene climate of SE Australia reconstructed from dust and river loads deposited offshore the River Murray Mouth. *Earth and Planetary Science Letters* 255: 257–272.

Gomez B, Carter L, Trustrum NA, Palmer A and Roberts A (2004) El Niño–Southern Oscillation signal associated with middle Holocene climate change in intercorrelated terrestrial and marine sediment cores, North Island, New Zealand. *Geology* 32: 653–656.

Griffiths ML, Drysdale R, Gagan MK, Zhao JX, Ayliffe LK, Hellstrom JC *et al.* (2009) Increasing Australian–Indonesian monsoon rainfall linked to early Holocene sea-level rise. *Nature Geoscience* 2: 636–639.

Guan H, Simmons CT and Love AJ (2009) Orographic controls on rain water isotope distribution in the Mount Lofty Ranges of South Australia. *Journal of Hydrology* 374: 255–264.

Haberle SG, Ledru M-P (2001) Correlations among charcoal records of fires from the past 16,000 years in Indonesia, Papua New Guinea, and Central and South America. *Quaternary Research* 55: 97–104.

Harrison SP (1993) Late Quaternary lake level changes and climates of Australia. *Quaternary Science Reviews* 12: 211–231.

Hellstrom J (2003) Rapid and accurate U/Th dating using parallel ion-counting multi-collector ICP-MS. *Journal Analytical Atomic Spectrometry* 18: 1346–1351.

Hellstrom J (2006) U–Th dating of speleothems with high initial 230Th using stratigraphical constraint. *Quaternary Geochronology* 1: 289–295.

Hendon HH, Thompson DWJ and Wheeler MC (2007) Australian rainfall and surface temperature variations associated with the Southern Annular Mode. *Journal of Climate* 20: 2452–2467.

Hesse PP, Magee JW and van der Kaars S (2004) Late Quaternary climates of the Australian arid zone: A review. *Quaternary International* 118–119: 87–102.

Hill KJ, Santoso A and England MH (2009) Interannual Tasmanian rainfall variability associated with large-scale climate modes. *Journal of Climate* 22: 4383–4397.

International Atomic Energy Agency (2001) *GNIP Maps and Animations*. Vienna: International Atomic Energy Agency, available from http://isohis.iaea.org

Johnson BJ, Miller GH, Fogel ML, Magee JW, Gagan MK and Chivas AR (1999) 65,000 years of vegetation change in central Australia and the Australian summer monsoon. *Science* 284: 1150–1152.

Keefer DK, Moseley ME and deFrance SD (2003) A 38 000-year record of floods and debris flows in the Ilo region of southern Peru and its relation to El Nino events and great earthquakes. *Palaeogeography, Palaeoclimatology, Palaeoecology* 194: 41–77.

Kim S, O'Neil JR (1997) Equilibrium and nonequilibrium isotope effects in synthetic carbonates. *Geochimica et Cosmochimica Acta* 61: 3461–3475.

Koutavas A, Lynch-Stieglitz J, Marchitto TM and Sachs JP (2002) El Nino-like pattern in ice age tropical Pacific sea surface temperature. *Science* 297: 226–230.

Lacelle D, Lauriol B and Clark ID (2007) Origin, age, and paleoenvironmental significance of carbonate precipitates from a granitic environment, Akshayuk Pass, southern Baffin Island, Canada. *Canadian Journal of Earth Sciences* 44: 61–79.

Lachniet MS (2009) Climatic and environmental controls on speleothems oxygen-isotope values. *Quaternary Science Reviews* 28: 412–432.

L'Heureux ML, Thompson DWJ (2006) Observed relationships between the El-Nino/Southern Oscillation and the extratropical zonal-mean circulation. *Journal of Climate* 19: 276–287.

Liu Z, Kutzbach J and Wu L (2000) Modeling climate shift of El Nino variability in the Holocene. *Geophysical Research Letters* 27: 2265–2268.

Magee JW, Miller GH, Spooner NA and Questiaux D (2004) Continuous 150 k.y. monsoon record from Lake Eyre, Australia: Insolation-forcing implications and unexpected Holocene failure. *Geology* 32: 885–888.

Markgraf V, Bradbury JP and Busby JR (1986) Paleoclimates in southwestern Tasmania during the last 13000 years. *Palaios* 1: 368–380.

Marx SK, McGowan HA and Kamber BS (2009) Long-range dust transport from eastern Australia: A proxy for Holocene aridity and ENSO-type climate variability. *Earth and Planetary Science Letters* 282: 167–177.

Mayewski PA, Rohling EE, Stager JC, Karlén W, Maasch KA, Meeker LD *et al.* (2004) Holocene climate variability. *Quaternary Research* 62: 243–255.

McCarthy L, Head L (2001) Holocene variability in semi-arid vegetation: New evidence from *Leporillus* middens from the Flinders Ranges, South Australia. *The Holocene* 11: 681–689.

McCarthy L, Head L and Quade J (1996) Holocene palaeoecology of the northern Flinders Ranges, South Australia, based on stick-nest rat (Leporillus spp.) middens: A preliminary overview. *Palaeogeography, Palaeoclimatology, Palaeoecology* 123: 205–218.

McCarthy D, Roger T and Casperson K (eds) (2006) *Floods in South Australia 1836–2005*. Bureau of Meterology, Commonwealth of Australia Government Publication, 252 pp.

McGlone MS, Kershaw AP and Markgraf V (1992) El Niño /Southern Oscillation climatic variability in Australasian and South American paleoenvironmental records. In: Diaz HF, Markgraf V (eds) *El Niño: Historical and Paleoclimatic Aspects of the Southern Oscillation*. Cambridge: Cambridge University Press, 436–462.

McGregor HV, Gagan MK (2004) Western Pacific coral $\delta^{18}O$ records of anomalous Holocene variability in the El Niño-Southern Oscillation. *Geophysical Research Letters* 31: 10.1029/2004GL019972.

McInnes KL, Suppiah R, Whetton PH, Hennessy KJ and Jones RN (2003) Climate change in South Australia, CSIRO Atmospheric Research. Available from: http://www.dar.csiro.au/publications/mcinnes_2003a.pdf

Meneghini B, Simmonds I and Smith I (2007) Association between Australian rainfall and the Southern Annular Mode. *International Journal of Climatology* 27: 109–121.

Mickler PJ, Stern LA and Banner JL (2006) Large kinetic isotope effects in modern speleothems. *Geological Society of America Bulletin* 118: 65–81.

Nicholls N (1992) Historical El Niño/Southern Oscillation variability in the Australasian region. In: Diaz HF, Makrkgraf V (eds) *El Niño: Historical and Paleoclimatic Aspects of the Southern Oscillation*. Cambridge: Cambridge University Press, 151–173.

Quigley M, Cupper M and Sandiford M (2006) Quaternary faults of south-central Australia: Palaeoseismicity, slip rates and origin. *Australian Journal of Earth Sciences* 53: 285–301.

Quigley M, Sandiford M and Cupper M (2007a) Distinguishing tectonic from climatic controls on range-front sedimentation. *Basin Research* 19: 491–505.

Quigley M, Sandiford M, Alimanovic A and Fifield LK (2007b) Landscape responses to intraplate tectonism: Quantitative constraints from ^{10}Be abundances. *Earth and Planetary Science Letters* 261: 120–133.

Quigley M, Sandiford M, Fifield K and Alimanovic A (2007c) Bedrock erosion and relief production in the northern Flinders Ranges, Australia. *Earth Surface Processes and Landforms* 32: 929–944.

Rodbell DT, Seltzer GO, Anderson DM, Abbott MB, Enfield DB and Newman JH (1999) A ~15,000-year record of El Niño-driven alluviation in southwestern Ecuador. *Science* 283: 516–521.

Saji NH, Goswami BN, Vinayachandran PN and Yamagata T (1999) A dipole mode in the tropical Indian Ocean. *Nature* 401: 360–363.

Sandweiss DH, Richardson JB, Reitz EJ, Rollins HB and Maasch KA (1996) Geoarchaeological evidence from Peru for a 5000 years B.P. onset of El Niño. *Science* 273: 1531–1533.

Schulmeister J, Lees B (1995) Pollen evidence from tropical Australia for the onset of ENSO-dominated climate at *c.*4000 BP. *The Holocene* 5: 10–18.

Schwerdtfeger P, Curran E (1996) Climate of the Flinders Ranges. In: Davies M, Twidale CR and Tyler M (eds) *Natural History of the Flinders Ranges*. Adelaide: Royal Society of South Australia Occasional Publication, 63–75.

Semenov EK, Sokolikhina EV and Sokolikhina NN (2008) Vertical circulation in the tropical atmosphere during extreme El Niño–Southern Oscillation events. *Russian Meteorology and Hydrology* 33: 416–423.

Singh G, Luly J (1991) Changes in vegetation and seasonal climates since the last full glacial at Lake Frome, South Australia. *Palaeogeography, Palaeoclimatology, Palaeoecology* 84: 75–86.

Sprigg RC (1984) *Arkaroola – Mount Painter in the Northern Flinders Ranges, S.A.: The Last Billion Years*. Arkaroola Pty Ltd.

Stanley P, De Deckker P (2002) A Holocene record of allochthonous, aeolian mineral grains in an Australian alpine lake: Implications for the history of climate change in southeastern Australia. *Journal of Paleoliminology* 27: 207–219.

Steig EJ (1999) Mid-Holocene climate change. *Science* 286: 1485–1487.

Suppiah R (1992) The Australian summer monsoon: A review. *Progress in Physical Geography* 16: 283–318.

Tudhope AW, Chilcott CP, McCulloch MT, Cook ER, Chappell J, Ellam RM *et al.* (2001) Variability in the El Niño–Southern Oscillation through a glacial–interglacial cycle. *Science* 291: 1511–1517.

Turcotte DL, Greene L (1993) A scale-invariant approach to flood frequency analysis. *Stochastic Hydrology and Hydraulics* 7: 33–40.

Ummenhofer CC, England MHP, McIntosh C, Meyers GA, Pook MJ, Risbey JS *et al.* (2009) What causes southeast Australia's worst droughts? *Geophysical Research Letters* 36: doi:10.1029/2008GL036801.

Wang P, Clemens SC, Beaufort L, Braconnot P, Ganssen G, Jian Z *et al.* (2005) Evolution and variability of the Asian monsoon system: State of the art and outstanding issues. *Quaternary Science Reviews* 24: 595–629.

Wells LE (1990) Holocene history of the El Nino phenomenon as recorded in flood sediments of northern coastal Peru. *Geology* 18: 1134–1137.

Williams GE (1973) Late Quaternary piedmont sedimentation, soil formation and palaeoclimates in arid South Australia. *Zeitschrift für Geomorphologie* 17: 102–125.

Williams M, Prescott J, Chappell J, Adamson D, Cock B, Walker K *et al.* (2001) The enigma of a late Pleistocene wetland in the Flinders Ranges, South Australia. *Quaternary International* 83–85: 129–144.

Wright W (1997) Tropical-extratropical cloudbands and Australian rainfall: I. Climatology. *International Journal of Climatology* 17: 807–829.

Xia QK, Zhao J-x and Collerson KD (2001) Early–mid Holocene climatic variations in Tasmania, Australia: Multi-proxy records in a stalagmite from Lynds Cave. *Earth and Planetary Science Letters* 194: 177–187.

Zhang X, Zwiers FW, Hegerl GC, Lambert FH, Gillett NP, Solomon S *et al.* (2007) Detection of human influence on twentieth-century precipitation trends. *Nature* 448: 461–465.